Ad-hoc information spread between mobile devices: a case study in analytical modeling of controlled self-organization in IT systems

Kamil Kloch[1], Jan W. Kantelhardt[2], Paul Lukowicz[1], Patrick Wüchner[3], Hermann de Meer[3],

[1] Embedded Systems Lab, University of Passau, Innstraße 43, D-94032 Passau Germany
[2] Institut für Physik, Martin-Luther-Universität Halle-Wittenberg, D-06099 Halle (Saale) Germany
[3] Computer Networks and Computer Communications, University of Passau, Innstraße 43, D-94032 Passau Germany

Abstract. We present an example of the use of analytical models to predict global properties of large-scale information technology systems from the parameters of simple local interactions. The example is intended as a first step towards using complex systems modeling methods to control self-organization in organic systems. It is motivated by a concrete application scenario of information distribution in emergency situations, but is relevant to other domains such as malware spread or social interactions. Specifically, we show how the spread of information through ad-hoc interactions between mobile devices depends on simple local interaction rules and parameters such as user mobility and physical interaction range. We show how three qualitatively different regimes of information 'infection rate' can be analytically derived and validate our model in extensive simulations.

1 Introduction

In this paper we present a specific example of the adaptation of an analytical complex system model to a self-organizing IT system. We show how logistic models from epidemiology can be applied to describe the spread of information or malware between mobile phones carried by people moving in a crowd. We derive the dependence of information penetration on crowd density, radio range, and motion speed. We show a 'phase transition'-like behavior: information is being spread with the speed either linearly increasing with the radio range, almost constant, or approximately exponentially. Another parameter-dependent emergent effect is the transition between local but dying 'information bubbles' and a continuous spread of information. The model is validated using extensive simulations showing good agreement with analytical predictions.
The value of the research presented in this paper is threefold:

First, on application level, it is part of a large, interdisciplinary EU project (SOCIONICAL, http://socionical.eu) to understand and exploit self-organization

in large-scale systems in which intelligent mobile devices interact with each other and with humans. A specific application scenario within the project is the study how sensing, communication, and cooperation between mobile devices (e.g., sensor enabled smart phones) can be used to steer crowd behavior in emergency situations (e.g., to speed up evacuation or prevent panic). Ensuring that information can be effectively spread between the devices in an ad-hoc fashion (infrastructure, even including mobile phones, cannot be assumed to work in such situations, as the case of the London subway bombings has shown) is a key requirement. Another obvious application of our model is the spread of malware through peer-to-peer interactions between mobile devices.

Second, on theoretical level, it extends previous approaches on information and virus spread (see [1,3,8,9] for related work) by specifically considering the effects of mobility and radio range. We provide an analytical solution for the 'infection ratio' (which is the key parameter in system description) and validate our results in extensive simulations.

Third, in the area of organic computing, so far little attention has been given to the use of analytical complex system models as means of understanding and controlling the evolution of self-organizing IT systems (see [5] for some discussion). The system that we are investigating is easily mapped to the corresponding model, as information spread is obviously closely related to the spread of disease. Nonetheless, it is a good initial example of a design where global properties and phase transitions can be analytically derived from the rules for simple local interactions. We see it as a first step in the direction of using analytical models as means of achieving control in self-organized systems.

2 The Scenario

This work is part of a large project to investigate **large-scale, complex interactions** between intelligent mobile devices and humans in their environment. In essence, it aims to apply models and concepts from complexity science and organic computing to ambient intelligence environments. Ambient intelligence research to date has concentrated on how individual intelligent devices interact with a single user or small groups of users. The questions that we ask include: How can such devices influence collective behavior? What sort of global effect can emerge from the coupled interactions and feedbacks between many different users and devices? How can we predict such global effects (and thus design systems in the sense of controlled emergence) from local interaction rules embedded in each individual device?

A key issue underlying many of the research questions that we are addressing is the spread of information. Assuming that devices forward information to others **in their physical proximity** according to certain rules: How will information spread on a global scale? Can we, in the sense of controlled self-organization, use simple control parameters like user mobility and interaction range to ensure (or prevent) rapid spread?

The specific application that has motivated this work is disaster management. For example, as described in a London Assembly Meeting Report[4], during the London subway bombings mobile phone communication broke down and lack of information has been a key problem for many of the people stuck inside the stations and trains. Thus, the ability to propagate information through the crowd in an ad-hoc fashion would have been of significant use. In more advanced scenarios that we are examining, phones are able to sense crowd motion and environmental conditions and propagate them throughout the crowd to optimize evacuation ([4]).

Other applications include social interactions (e.g., 'flash mobs'), media distribution and the spread of malware.

2.1 Model Assumptions

For the simulation and modeling, some simplifying assumptions have been made. All mobile agents (representing, e.g., persons with cellular phones) are placed in a square board of a fixed size. To reduce the boundary effect of agents hitting the walls, the sides of the square are wrapped left-to-right and up-to-down (periodic boundary conditions), so that the actual simulation is being carried out on a torus.

At the beginning, the agents are placed uniformly on the board and only a fraction of agents has some interesting information or malware to be spread (status: **infected**), while all others are initially uninfected. The direction of motion of each agent is chosen randomly. Each agent moves along a straight line for a random number of steps. The length of the straight paths varies randomly from a few steps to half the size of the board. After that, the direction of the agent and the length of its straight path is randomly changed, and the procedure is repeated. The achieved motion is random and – at the same time – resembles the movement of agents in a crowd.

Each mobile agent carries a mobile device and is surrounded by the device's radio range. The radio range is modeled by a flat disc. If an uninfected device collides with the radio range of an infected device, it will also get infected immediately and change its status to infected. With a certain probability, in each simulation step, an agent will reset its infected mobile device, and thus, will get rid of the infection without getting immune.

The model parameters can be summarized as follows: (1) number of agents: N (since it is assumed that all agents carry only one device, N is equal to the number of devices), (2) initial infection ratio: $I \in [0 \dots 1]$ (probability that a device will be infected initially), (3) system length: L unit lengths (overall area of $L \times L$ square unit lengths under consideration, kept constant in the presented scenario), (4) radio (interaction) range: R, (5) velocity of agents: v (in unit lengths per simulation step), and, optionally, (6) device reset probability: $P \in [0 \dots 1]$ (probability that an agent will reset its infected mobile device within a simulation step).

[4] see `http://www.london.gov.uk/assembly/resilience/2005/77reviewdec01/minutes/transcript.pdf`

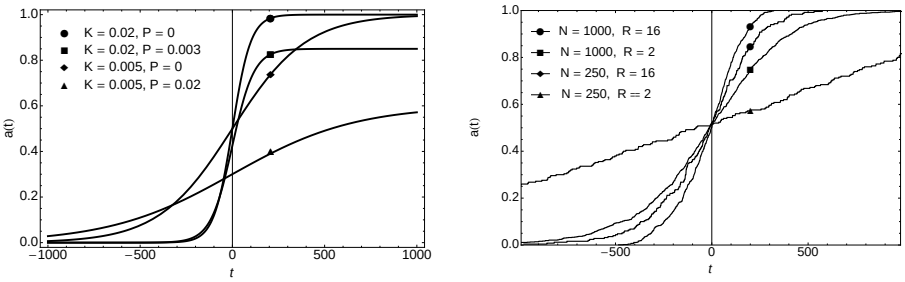

(a) (b)

Fig. 1. (a): Plotting $a(t)$ against t for $T = 0$ and different values of K and P. (b): Relative number of infected devices $a(t)$ versus simulation steps t for various number N of agents and radio ranges R. The plot illustrates the definition of the time scale.

2.2 Logistic Model

A common model for the spread of diseases is the logistic model (see, e.g., [2]). This model also gets more and more attention from researchers in the field of computer science and engineering (see, e.g., [6] and [7]). In our scenario, the logistic equation takes the following form:

$$a'(t) = K\,a(t)\,(1 - a(t)) - P\,a(t). \tag{1}$$

Equation (1) can be motivated as follows. The maximum change in the infection ratio $a(t)$ $(0 \leqslant a(t) \leqslant 1)$ within an infinitesimal time interval around time t is given by the number of infected agents $a(t)$ at time t times the infection ratio K. Thus, K is the unimpeded infection rate that applies to the case when $P = 0$ and there is only one infected agent, and hence, each collision of this agent that occurs during the time interval leads to a new infection. The maximum change is delimited by the saturation effect caused by the finite number of agents to be infected, modeled by the factor $(1 - a(t))$ and by the number $P\,a(t)$ of infected agents that reset their device within the time interval.

By solving the differential equation (1) we get

$$a(t) = \frac{K - P}{K\left(1 + e^{-(K-P)(t-T)} - Re^{-(K-P)(t-T)}\right)},$$

where T is the location parameter that fixes the time when 50% of all agents is infected, i.e., $a(T) = 0.5$, in the case $P = 0$. In Fig. 1(a), $a(t)$ is plotted against time t for $T = 0$ and various values of K and P according to (1).

The slope of the logistic curves shown in Fig. 1(a) at $t = 0$ can be obtained from (1):

$$a'(0) = K\,a(0)\,(1 - a(0)) - P\,a(0) = K/4 - P/2. \tag{2}$$

Thus, knowing the value P, K can be obtained by investigating the slope of the curves at $t = 0$. The fix points are the expected values of $a(t)$ in steady state

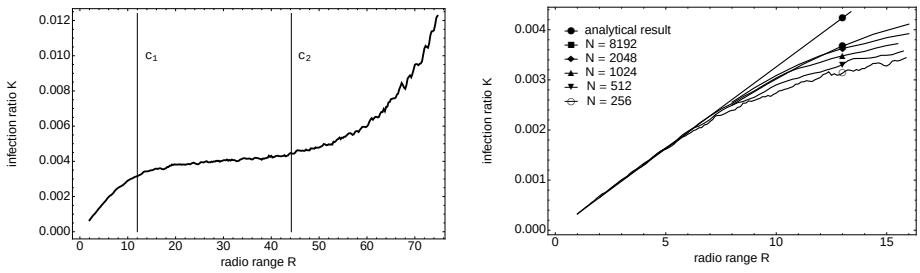

(a) (b)

Fig. 2. (a): Simulation results: infection ratio K plotted versus radio range R for $N = 512$, $L = 2000$ and $2 \leqslant R \leqslant 75$. Vertical lines c_1 and c_2 mark the separations of the three regimes. (b): First regime – scaled simulation results for various N compared with the analytical value of K computed according to (4).

$t \to \infty$, i.e., $a'(t) = 0$. In our case, $\lim_{a\to\infty} a(t) = (K - P)/K$. This value can be used to determine a suitable value for P depending on K. However, computing K by running simulations for each possible parameter set is unsatisfactory. In the following we deal with the primary concern of the paper, that is, achieving the closed-form equation for K that is based merely on scenario's parameters.

3 Model and Simulation

For the evaluation, the relative number $a(t)$ of infected devices at time t (simulation step) is of main interest. In Fig. 1(b), $a(t)$ is plotted versus t for four simulation runs with various values of N. The other model parameters are chosen as follows. The initial infection ratio I is chosen equal to $1/N$, which means one infected agent. The devices' radio range R is fixed to 10 unit lengths. The velocity v of the agents is one unit length per time unit. The time axis (horizontal axis) is chosen such that $a(0) = 0.5$. It can be seen that all curves show qualitatively the same behavior. However, the quantitative slope of the curves depends on the number of agents. Actually, as it will be shown later in more detail, the slope depends on the density of agents $\rho = N/L^2$ and on the system parameters that are kept constant in Fig. 1(b), like the agents' speed v and the radio range R.

In the following, we focus on the case $P = 0$ and $I = 1/N$, i.e., devices are not reset and exactly one device is initially infected. Figure 2(a) depicts the results of the simulation for 512 agents, radio ranges varying from 2 to 75, board size $L = 2000$, and velocity $v = 1$. The calculated values of the unimpeded infection ratio K, depicted on the vertical axis, are obtained from (2). For each value of R, the median of the slope $a'(0)$ at $t = 0$ is obtained from polynomial approximations for 50 simulation runs.

Simulation results shown in Fig. 2(a) reveal three distinct regimes with different dependences of the parameter K on R. At first, the infection ratio K

grows linearly with radio range R. In the second regime the value of K remains almost constant. This is a very surprising result. Finally, in the third regime, the infection ratio starts to grow very rapidly with R. The three regimes are analyzed and described analytically in the following sections.

3.1 First scaling regime

In the first regime, we consider the case of very small radio ranges. Thus, agents travel long distances between coming into contact with each other and the infected and uninfected agents are typically spread uniformly across the board (see Fig. 3(a)). In order to derive the R dependence of K, we note that the unimpeded infection rate K specifies the expected number of new infections per time unit if no reset is involved. Hence, each collision of an infected agent with another agent has a high probability to cause a new infection, since the other agent is usually uninfected. By collision we mean that the distance between the two agents becomes as small as R. To calculate the expected number of collisions within one time step, we adapt the mean free path approach well-known from the kinetic theory of gases for a two-dimensional setting, agents of different sizes, and non-negligible radius of infected agents.

Consider an infected agent moving along a straight path with speed $\bar{v}$. During the next time unit the agent's radio range R will reach a previously untouched area of size $\bar{v} \cdot 2R$. All previously uninfected agents in this area will then be infected. The mean number of agents in the area is given by its size times the mean density of agents,

$$K = (\bar{v} \cdot 2R)\, N/L^2. \tag{3}$$

Note that $\bar{v}$ is not equal to the infected agent's velocity v in general, since both, infected and uninfected agents, are moving. Since in the presented scenario also the uninfected agents move randomly, $\bar{v}$ has to be calculated as the expected relative velocity of the uninfected agents with respect to the infected agent.

Therefore, we consider a reference system in which the infected agent is at rest. Without loss of generality, we can assume that it is moving to the right with velocity $\boldsymbol{v}_1 = (v, 0)$ (the two components of the vector indicating the speeds in x and y direction, respectively). In the considered moving reference system, the speed of the uninfected agents is thus given by $\boldsymbol{v}(\varphi) = \boldsymbol{v}_2 - \boldsymbol{v}_1 = v\,(\cos\varphi - 1, \sin\varphi)$ where $0 \leqslant \varphi < 2\pi$ denotes the (random) direction of motion of the uninfected agent in the original resting reference system. Consequently, the average absolute value of $\boldsymbol{v}$ is equal to

$$\begin{aligned}\bar{v} &= \frac{1}{2\pi}\int_0^{2\pi} |\boldsymbol{v}(\varphi)|\, d\varphi = \frac{1}{2\pi}\int_0^{2\pi} v\,\sqrt{(\cos\varphi - 1)^2 + \sin^2\varphi}\, d\varphi \\ &= \frac{v}{2\pi}\int_0^{2\pi} \sqrt{2 - 2\cos(\varphi)}\, d\varphi = \frac{4v}{\pi} \approx 1.2732 \cdot v.\end{aligned}$$

Hence, the unimpeded infection rate K can be calculated based on (3):

$$K = 8vR\rho\pi \approx 2.5465 \cdot vR\rho. \tag{4}$$

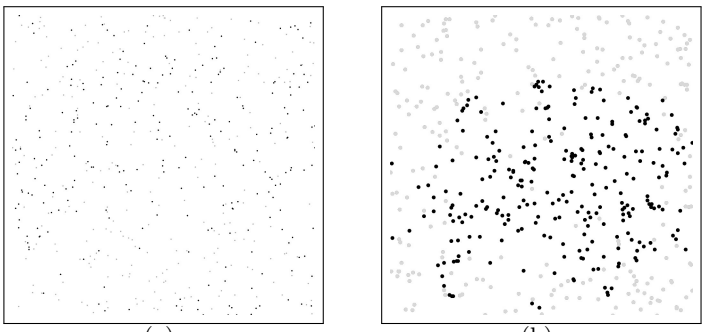

(a) (b)

Fig. 3. Cross-over c_1 between the first and the second regime for 512 agents, infection ratio $a(0) = 0.5$, $R = 8$ (a) and $R = 20$ (b).

Fig. 2(b) shows a comparison between the simulation and the analytic result for several parameter settings. While keeping the size of the simulated area ($L = 2000$) constant, the number N of agents and the radio range R are varied. N varies from 256 (low density) to 8192 (highly crowded area). Each point in Fig. 2(b) represents the median of 50 simulation runs. For $N \neq 512$ the results on the horizontal axis have been scaled linearly with respect to ρ so that the analytical results derived from (4) are the same. The straight line depicts our analytical result based on the mean-value approach.

For $N = 512$ and radio ranges $R < 9$, the analytical model yields almost perfect results. Simulations confirm the linear growth of the infection ratio K with radio range R and agents' density ρ. Around $R = 10$ (for $N = 512$), the value of K ceases to grow linearly with R and we observe the crossover to the second regime with almost constant K.

The phase transition at c_1 (between the first and the second regime) can be understood by taking a look at the results of two experiments for 512 agents, with $R = 8$ and $R = 20$, respectively. Figure 3 shows the distribution of the agents at the time when half of the population is infected. This is the moment which determines the value of K (recall (2)). For $R = 8$, the infected agents are scattered across the entire board. For $R = 20$, they tend to conglomerate. Most of the infected agents are then surrounded by others which are infected as well, and thus, the number of agents to be infected in the next time stepts is much smaller.

3.2 Second scaling regime

With increasing radio range of the devices, the infected agents cease to be uniformly distributed across the entire board and our analytic description for the first regime fails. Instead, the agents tend to form a disk-like pattern (see Fig. 3). This behavior becomes more pronounced for larger values of R, for which the infected agents form an almost perfect disk growing linearly with time.

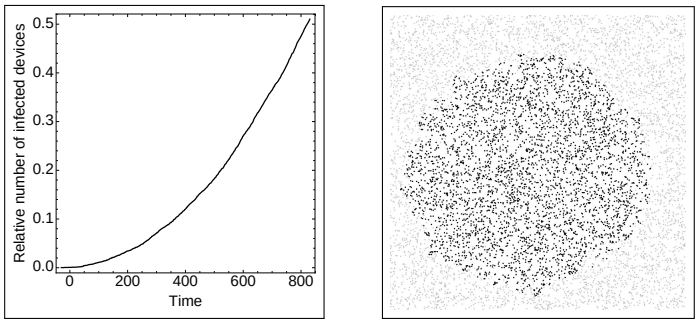

Fig. 4. Second regime: simulation run confirming the analytical model.

We denote by $a(t)$ the relative number of the infected devices at iteration step t. Now, recall from Sec. 2.2 that parameter K is determined by the slope of $a(t)$ at the point $t = t_0$ such that $a(t_0) = 0.5$. We combine this fact with the knowledge about the distribution of the infected agents to develop the following analytical model. Firstly, we assume that at iteration step t_0 for which $a(t_0) = 0.5$ the infected agents form a disk D of radius r_D. Since all agents are distributed uniformly across the entire board, the area of D is half of the board's size, i.e.,

$$\pi\, r_D^2 = L^2/2, \tag{5}$$

which yields $r_D \approx 0.4\, L$. The second assumption is a crucial one: the radius of the disk formed by the infected agents at time t for $t \leqslant t_0$ is approximately equal to $v \cdot t$, i.e., the distance travelled by a single agent in t steps. In particular, this implies that

$$r_D = t_0\, v \quad \text{and} \quad a(t) = c \cdot t^2, \text{ for some constant } c \text{ and } t \leqslant t_0. \tag{6}$$

Both assumptions we have made are supported by the simulation results and follow from the special property shared by the radio ranges considered in the second regime: they are big enough to guarantee the compact, disk-like form of the infected agents, yet small enough not to cause chain infections and thus retaining agents' velocity as the prevailing factor of virus spread.

From (2), (5), (6) and the fact that $a(t_0) = 0.5$ we now get

$$K = 4\, a'(t_0) = 4 \cdot 2\, c\, t_0 = 8\, \frac{0.5}{t_0^2}\, t_0 = \frac{4}{t_0} = \frac{4\, v}{r_D} = \frac{4\sqrt{2\pi} v}{L} \approx \frac{10v}{L}. \tag{7}$$

The simulation run for $L = 2000$, $N = 8192$, $R = 10$, and $v = 1$ shown in Fig. 4 confirms this analytical model. Infection ratio grows quadratically with time, reaches 50% for $t_0 = 840$ and the infected agents form a disk of radius ≈ 800.

The position of the first crossover c_1 (see Fig. 2(a)) separating regimes one and two can be approximated by equating Eqs. (4) and (7). This yields

$$K = \frac{8 v R_{c_1} N}{\pi L^2} = \frac{4\sqrt{2\pi} v}{L} \qquad \Longrightarrow \qquad R_{c_1} = \sqrt{\frac{\pi^3}{2}}\, \frac{L}{N} \approx 3.937\, \frac{L}{N}. \tag{8}$$

We see that the position of c_1 depends linearly on L/N.

3.3 Third scaling regime

The crossover c_2 from the second (nearly constant) regime to the third regime (see Fig. 2(a)) occurs when the mean distance between the agents becomes comparable with R. Then, immediate chain infections can occur, if a third agent happens to be within the radio range of the second (just infected) agent, even if it is not sufficiently close to the first (originally infected) agent.

The value of the crossover length R_{c_2}, i.e., the position of crossover c_2, can be calculated analytically as follows. Firstly, we have to determine the mean distance between nearest neighbor agents. Placing the agents randomly on the board can be interpreted as a Poisson process. Recall that a Poisson distribution is typically used to describe the probability of the occurrence of uncorrelated events over time, space, or length. Our use of the Poisson distribution is justified by the fact that the random locations of the agents are independent. The number n of agents within a given area A is described by the probability function

$$F(n) = \frac{(\rho A)^n}{n!} e^{-\rho A}, \text{ for } n = 0, 1, \ldots .$$

We fix the position of a single agent p. Since the agents are independent, the probability that there is no other agent within distance r from p is given by $F(0) = \exp[-\rho\,\pi r^2]$. If x is the distance of the nearest agent from p, the probability that $x \leqslant r$ is equal to $P(x \leqslant r) = 1 - P(x > r) = 1 - F(0) = 1 - \exp[-\rho\,\pi r^2]$. Consequently, the density function of the distance from p to its nearest neighbor is given by

$$f(r) = \frac{dP(x \leqslant r)}{dr} = \frac{d}{dr}\left(1 - e^{-\rho\,\pi r^2}\right) = 2\pi\,\rho\,r\,e^{-\rho\,\pi r^2},$$

Finally, the mean nearest neighbor distance d_p is equal to

$$d_p = \int_0^{+\infty} f(r)\,r\;dr = \frac{1}{2\sqrt{\rho}} = \frac{L}{2\sqrt{N}} = R_{c_2}, \tag{9}$$

with L and N denoting system size and the number of agents, respectively.

The characteristic length scale d_p determines analytically the crossover c_2 from regime two to regime three, where chain reactions start to occur. It is therefore denoted by R_{c_2} in (9). We note that R_{c_2} scales with $L/\sqrt{N}$, while R_{c_1} scales with L/N, see (8). Figure 5 shows the results of our simulations, i.e. the infection ratio K, versus the scaled radio range R/d_p for four numbers N of agents and systems of length $L = 2000$. The scaling behavior is clearly confirmed. The curves in the third regime, i.e., for $R/d_p > 1$, differ just by a constant offset which is due to different absolute values occurring already in the second regime (for $R/d_p < 1$).

In general, the value of K in the second regime given by (7) for $L = 2000$ and $v = 1$ is $K = 0.05$. Figure 5 shows that this threshold is not fully reached in our simulations for smaller densities $\rho = N/L^2$. In particular, K does not exceed 0.03 before the onset of the third regime at $R = R_{c_2}$ if $N = 256$. The reason is

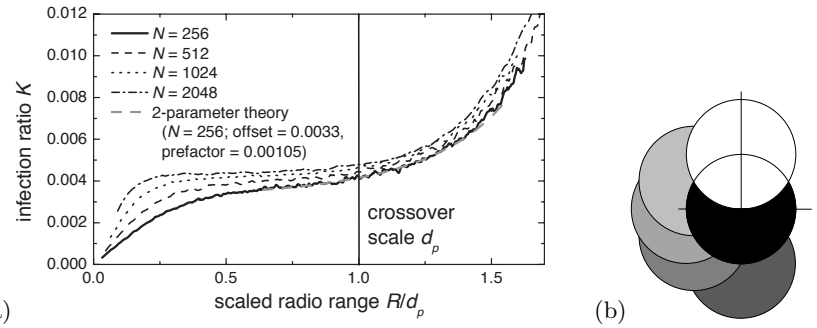

Fig. 5. (a) Scaling plot for the infection ratio K in the third regime. The K values for different N (see legend) and $L = 2000$ are plotted versus the scaled radio range R/d_p with d_p taken from (9). The numerical curves are parallel with a small offest in the third regime ($R/d_p > 1$). The dashed grey line shows the analytic theory. Two fitting parameters are needed: a prefactor and an offset; both will be different for $N > 256$. (b) Illustration of the geometical constraint determining chain infections for simultaneous infection of three agents.

the closeness of both crossovers for small ρ (and N). While the second regime is rather broad for $N = 2048$, it nearly vanishes for $N = 256$, where

$$\frac{R_{c_1}}{R_{c_2}} = \left(\sqrt{\frac{\pi^3}{2}}\frac{L}{N}\right) / \left(\frac{L}{2\sqrt{N}}\right) = \sqrt{2\pi^3/N} \approx 0.492$$

compared with $R_{c_1}/R_{c_2} \approx 0.174$ for $N = 2048$. Therefore, $K = 0.05$ is not fully reached for the lower values of N, and the curve in the third regime is consequently shifted downwards by a small amount as seen in Fig. 5. This, however, does not devaliate our analytical descriptions of both crossovers nor the unified scaling behavior seen in the third regime.

To derive the form of the scaling curve for $R/d_p > 1$ in Fig. 5, we have to consider the geometric constraints for immediate chain infections. The probability of a chain infection is not related with the motion of the agents. Therefore, one need not consider trajectories, and the analysis is mainly geometrical. A newly infected (second) agent is always located at distance R from the infecting agent, since it would have been infected earlier otherwise. Its radio range, i.e., the area in which a third agent could be infected, thus overlaps with the radio range area A_1 of the first agent (where no additional third agent could be infected). This extended radio range area A_2 is thus not a circle. Nevertheless, the corresponding area can be calculated analytically. Figure 5(b) illustrates A_1 (white) and A_2 (black). Without loss of generality, we assume that A_2 is to the right of A_1. A_2 is a half circle ($\pi/2\,R^2$) plus twice the (nearly triangular) part with height $R/2$ and length R; its exact area is $2.18918\,R^2$. The additional infection probability (first order term) is thus $F_1 = 2.18918\,\rho\,R^2$.

However, the chain reaction can go on, since there could be a fourth agent in the radio range of the third agent. Since the third agent can be anywhere in A_2 (black), different areas A_3 for the forth agent must be considered depending on the actual position of the third agent. Figure 5(b) illustrates several possibilities, for which we have calculated the area analytically (grey). All of these circles have the center on the edge of the black area. However, positions closer to the center of the black area are also possible. To take them into account in a reasonable averaging procedure, one must note that the range of possible centers for A_3 increases by r with the distance r from the center of A_2. A corresponding well-justified (although not analytically exact) averaging procedure yields $1.34331\,R^2$ for the average area A_3. The probability of the second order spontaneous infection is thus proportional to the product of first order $2.18918\,\rho\,R^2$ times $1.34331\,\rho\,R^2$, yielding $F_2 = 2.94076\,\rho^2\,R^4$ for the second term. Extending this rule further, we have approximated the third term by $F_3 = 3.63601\,\rho^3\,R^6$, etc.

The analytical curve included in Fig. 5 is furthermore based on approximations of the forth and fifth terms F_4 and F_5, which we also approximated. Clearly, a fast convergence of this series $F = F_1 + F_2 + F_3 + F_4 + F_5 + \ldots$ requires that $\rho R^2 \ll 1$. This is violated for large R or ρ of course. The calculation thus becomes inaccurate for large radio ranges R and large densities $\rho = N/L^2$. In particular, not taking into account terms for very large order (and stopping with F_5) will lead to K values which are too small for large R.

Figure 5 shows that data from the simulation of $N = 256$ can be fitted very well. We have to employ two fit parameters: the constant level in the second regime and a prefactor relating F to K,

$$K = \text{offset} + \text{prefactor}\,F. \tag{10}$$

The fit is very good except for very large R as expected. We note that the value of the offset parameter in (10) is close to the constant $K = 0.05$ in the second regime given by the analytic (7). It is somewhat lower for small N due to the shortness of the second regime as explained above. Therefore, the offset is not a real fitting parameter. In addition, the prefactor in (10) is related to the ratio of the mean velocity $v \approx 1.2732$ (see calculation for first regime) over the board length $L = 2000$, and thus also not a real fitting parameter. Again, the numerical values obtained for the fit in Fig. 5 deviate due to the specificity of the second regime. The deviations are less for larger values of N, where the same analytical theory with two fitting parameters applies although both parameters in (10) are slightly different.

4 Conclusion

We have shown that depending on the physical interaction range and the average speed of physical motion there are three distinct regimes for the information distribution rate. The proposed analytical model comprises both the three regimes and the two cross-overs between them:

(i) Phase of linear growth (see Sec. 3.1). For small radio ranges R and low density ρ of agents the infection ratio K is proportional to $R\rho$. The position of the first cross-over depends linearly on L/N.
(ii) Phase of an almost constant value of K, more pronounced for larger densities (see Sec. 3.2). Radio ranges are big enough to prohibit a homogenous distribution of infected agents, yet small enough not to cause a chain infection. In our analytical model, we prove that the value of K indeed does not depend on R. The second cross-over is determined by the mean distance between the agents and thus scales with $L/\sqrt{N}$.
(iii) Phase of a very rapid growth of K, when radio ranges are big enough to trigger chain infections (see Sec. 3.3). The probability of a chain infection is not related with the motion of the agents and indeed, in the obtained analytical model the value of K depends only on R and ρ.

Our models have made some simplifying assumptions (e.g., torus topology, random motion, and homogeneous distribution) so that applicability to real life emergency situations needs to be further investigated in more advanced simulations. However, the results are a good indication of the type of behavior that can be expected to occur. Most of all, the work is an initial example of how analytical complex systems models can be leveraged to facilitate control and predictability in large-scale organic systems.

References

1. T. Arai, E. Yoshida, and J. Ota. Information diffusion by local communication of multiple mobilerobots. *Systems, Man and Cybernetics, 1993.'Systems Engineering in the Service of Humans', Conference Proceedings*, pages 535–540, 1993.
2. Nino Boccara. *Modeling Complex Systems*. Springer-Verlag, 2004.
3. Z. Chen, L. Gao, and K. Kwiat. Modeling the spread of active worms. *INFOCOM 2003. Twenty-Second Annual Joint Conference of the IEEE Computer and Communications Societies. IEEE*, 3, 2003.
4. A. Ferscha and K. Zia. Lifebelt: Silent directional guidance for crowd evacuation. In *IEEE ISWC09*, 2009.
5. K. Mainzer. Organic Computing and Complex Dynamical Systems Conceptual Foundations and Interdisciplinary Perspectives. *Organic Computing*, page 105, 2008.
6. David M. Nicol and Michael Liljenstam. Models of active worm defenses. In *Proc. of Measurement, Modeling and Analysis of the Internet Workshop (IMA'04)*, 2004.
7. Stuart Staniford, Vern Paxson, and Nicholas Weaver. How to own the internet in your spare time. In *Proceedings of the 11th USENIX Security Symposium*, pages 149–167, Berkeley, CA, USA, 2002. USENIX Association.
8. Cliff Changchun Zou, Weibo Gong, and Don Towsley. Code red worm propagation modeling and analysis. In *CCS '02: Proceedings of the 9th ACM conference on Computer and communications security*, pages 138–147, New York, 2002. ACM.
9. Cliff Changchun Zou, Weibo Gong, and Don Towsley. Worm propagation modeling and analysis under dynamic quarantine defense. In *WORM '03: Proceedings of the 2003 ACM workshop on Rapid malcode*, pages 51–60, New York, 2003. ACM.